Available online at www.sciencedirect.com

ScienceDirect

Solar Energy 115 (2015) 180–194

SOLAR ENERGY

www.elsevier.com/locate/solener

Experimental and computational study of thermal energy storage with encapsulated $NaNO_3$ for high temperature applications

Ying Zheng [a], John L. Barton [a], Kemal Tuzla [a,*], John C. Chen [a], Sudhakar Neti [b], Alparslan Oztekin [b], Wojciech Z. Misiolek [c]

[a] Chemical and Biomolecular Engineering, P.C. Rossin College of Engineering and Applied Science, Lehigh University, Bethlehem, PA 18015, USA
[b] Mechanical Engineering and Mechanics, P.C. Rossin College of Engineering and Applied Science, Lehigh University, Bethlehem, PA 18015, USA
[c] Materials Science and Engineering, P.C. Rossin College of Engineering and Applied Science, Lehigh University, Bethlehem, PA 18015, USA

Received 20 September 2014; received in revised form 15 December 2014; accepted 5 February 2015

Communicated by: Associate Editor Halime Paksoy

Abstract

The objective of this work is to establish methods for storage of thermal energy using encapsulated phase change materials (EPCMs) at temperatures up to 440 °C applicable in concentrating solar plants (CSPs), in which heat transfer fluid (HTF) from the solar collector would pass through the storage system embedded with EPCM capsules. $NaNO_3$, having latent heat of 176 kJ/kg at 308 °C, is selected as the storage medium. Stainless steel capsules containing $NaNO_3$ are fabricated and installed in a pilot-scale thermal energy storage (TES) system for performance tests. Compressed air is used as heat transfer fluid in the current tests. The test section (T/S) with EPCM capsules successfully demonstrate the ability to transfer thermal energy to and from a transport fluid, achieving energy storage and retrieval in multiple charging and discharging cycles. In a given cycle where capsule temperatures varied from ~250 °C to ~386 °C, the EPCM is found to store significant energy per unit mass (~211 kJ/kg of capsule), with the phase change material (PCM) $NaNO_3$ accounting for ~95% of the total energy stored in the capsules. The latent heat of the $NaNO_3$ contributes to ~42% of the energy stored in the capsules. It is expected that the storage density of the EPCM would be even greater for plant size TES systems with larger size capsules, without the penalties associated with the limited scale used here. A mathematical model has been developed for the test section with EPCM capsules and its predictions are found to agree with experimental measurements within 7% discrepancy in stored energy. The dynamic performance of charging and discharging rates are also well predicted by the model, giving confidence for engineering design capabilities in future applications using EPCMs for thermal energy storage.

Keywords: Thermal energy storage; Encapsulated phase change material; Latent heat storage; High temperature solar applications; $NaNO_3$; Concentrated solar plants

1. Introduction

Renewable energy is of considerable current interest due to increasing demands on the world's supply of fossil fuels, and world-wide attention on global warming associated with the increasing amount of CO_2 in our atmosphere, as noted by latest declarations from the Intergovernmental Panel on Climate Change (Metz et al., 2005). To date, renewable sources have only been minor contributors to the worlds energy supply. In 2011, approximately 13% of the total electricity generation in US was derived from renewable energy sources, with solar energy accounting for ~1% (Energy Information Administration, 2012b).

* Corresponding author. Tel.: +1 610 758 4729; fax: +1 610 758 5057.
E-mail address: kt01@lehigh.edu (K. Tuzla).

http://dx.doi.org/10.1016/j.solener.2015.02.002
0038-092X/

Nomenclature

ΔH	latent heat (kJ/kg)
Δr	radius step (m)
Δt	time step (s)
Δx	step in x axis (m)
A	surface area of per unit volume of unit cell (m^2/m^3)
Cp	heat capacity (J/kg °C)
G	flow flux (kg/m^2 s)
h	convective heat transfer coefficient (W/m^2 s)
k	thermal conductivity (W/m °C)
L	length (m)
m	mass (kg)
$\dot{m}$	mass flow rate (kg/s)
Q	energy change (J)
$\dot{Q}$	rate of energy change (W)
r	radius (m)
S	displacement of the melting front (m)
t	time (s)
x	location in x axis (m)
z	elevation (m)
δ	thickness (m)
ρ	density (kg/m^3)

Subscripts

a	ambient
Capsules	capsules include the encapsulated materials and encapsulation shells
Copper	copper capsules
c	chamber of test section
f	heat transfer fluid
in	at the inlet of test section
j	at location j
l	heat losses
out	at the outlet of test section
PCM	phase change material
s	shell of the capsule
t	at time t
t_0	at time t_0

Acronyms

CSP	concentrating solar plant
EPCM	encapsulated phase change material
HTF	heat transfer fluid
PCM	phase change material
TES	thermal energy storage
T/S	test section

One disadvantage of most renewable sources, including solar energy, is their intermittent and variable nature as they are governed by locations and weather conditions. Even in locations with favorable solar incidence, the diurnal cycle provides only about 3000 h of significant irradiance in a year. Consequently, current solar power plants have average capacity factors of barely 20%, in comparison to capacity factors of 85% for conventional coal plants and 90% for advanced nuclear power plants (Energy Information Administration, 2012a). One way to improve the capacity factor of solar plants is to integrate a thermal energy storage system in the power plants. Such systems enable the storage of energy when the solar incidence is strong, and then release that energy for power generation during cloudy or nocturnal periods of low or no solar incidence. It has been reported that the use of storage systems can double the capacity factor of the solar thermal/electric power plants to ~40% or greater (Kuravi et al., 2013).

There are three mechanisms for thermal energy storage: sensible heat, latent heat, and thermo-chemical energy. Compared with thermo-chemical energy storage, sensible energy storage systems and latent heat storage systems, which utilize the reversible enthalpy changes of a storage medium, are thermodynamically attractive and economically promising. Several concentrating solar plants have been built with two-tank TES systems (Dunn et al., 2012), where the energy is stored by sensible heating of molten salt, and the molten salt is stored and circulates between a cold tank and a hot tank. In daytime with excess sunshine, the molten salt is pumped through a heat exchanger to capture the energy from a heat transfer fluid (HTF), such as oil, and store the energy in the hot tank. When the energy is needed, the molten salt is pumped from the hot tank to release the energy to the HTF in a heat exchanger, and then circuit back to the cold tank. A one-tank TES system with hot fluid at the top and cold fluid at the bottom of the tank, was developed by Sandia National Laboratories, using quartzite rock and silica sand as the storage medium (Pacheco et al., 2002). Such one-tank TES system using sensible heating of the storage medium was predicted to reduce the investment of the storage system by ~32% compared to the two-tank system (Dunn et al., 2012). However, large solar plants would need TES components of 500 MW h thermal, or greater, requiring large volumes of storage medium, of the order $\sim 5 \times 10^5$ m^3. Latent heat storage, which utilizes latent heat of phase change to complement sensible heat storage, can achieve significantly higher storage densities (IRENA, 2013), thus reducing the required volume of storage medium and its containment vessel. This promises to significantly reduce the capital cost of TES, and the total cost of solar electric generating plants.

A few research and development efforts have pioneered the use of latent heat storage technology at temperatures suitable for CSPs. Several reports has been focused on a shell-and-tube system, with the phase change materials,

such as KNO_3, placed in a large container and a heat transfer fluid flowing in the embedded tubes in the PCM (Dinter et al., 1991; Michels and Pitz-Paal, 2007; Kuravi et al., 2013). A difficulty of such shell-and-tube system is its slow charging and discharging rates, which are due to the low thermal conductivity of most PCMs and limited heat transfer area of the immersed tubes. This is of special concern during the heat extraction (discharging) phase when liquid PCM would form a frozen layer on the heat transfer surfaces, hampering further energy transfer between PCM and the heat transfer fluid (HTF).

To address this issue, three different approaches have been identified (Steinmann et al., 2010): (a) encapsulation of the storage material to limit the average distance for heat transfer; (b) addition of a substance to the PCM to create a composite material with high thermal conductivity; and (c) integration of heat transfer structures, such as fins (Laing et al., 2013) to ensure sufficient heat transfer between PCM and HTF. The approach investigated in the current development is to reduce the dimensional scale of the PCM by containing measured amounts of the PCM in individual capsules, of which the approach has been proposed in early 1988 by Luz International Ltd. et al. (1988). By placing limited amounts of the PCM in individual capsules, one minimizes the dimensional scale for conduction path within the PCM, and simultaneously increases the total contact area of the capsules for convective heat transfer with the HTF. With appropriate selection of the capsules' dimensions, the physical scale for heat transfer can be optimized to reduce conduction resistance within the PCM and to enhance external convective heat transfer between the capsules and the HTF. The ideal dimensions for the capsules can be optimized for various PCMs and HTFs with different thermal properties. In plant applications, this beneficial improvement of heat transfer would be balanced against fabrication cost of encapsulation. Initial cost estimates indicated that these types of EPCM based TES system can be implemented with a less expensive investment than currently used two-tank system for storage of thermal energy (Zheng et al., 2013; Zhao et al., 2012).

Several issues need to be resolved for the proposed use of encapsulated PCMs for thermal energy storage in CSP: (1) Selection of a PCM for operating temperatures up to 440 °C; (2) Selection of an encapsulation material, compatible with the PCM; (3) Dimensional optimization of the capsules for heat transfer, as described above; (4) Characterization of the encapsulated PCM, and evaluation of its storage performance in long-term melting/freezing cycles.

All four issues have been addressed in recent development work and the solutions are described in several reports and publications (Zheng et al., 2013; Zhao et al., 2012; Blaney et al., 2013). The present work follows these precursor developments by actually designing, operating, and testing a pilot-scale TES system with EPCMs. To verify that such a system can be successfully engineered, a computer simulation model of the EPCM based TES system is also developed and its predictions compare to actual measurements of performance.

2. Design, operation and energy measurements of the EPCM based TES system

In previous research for identification of qualified encapsulated phase change materials, $NaNO_3$ and cylindrical stainless steel capsule was found to be compatible with the $NaNO_3$ in long-term thermal cycling (Zheng et al., 2013). These investigators illustrated that the storage capacity has not been deteriorated under repeated thermal tests in a specially-made calorimeter. The present work is aimed to establish a method for storage of thermal energy utilizing encapsulated PCM and demonstrate its technical and economic feasibilities through testing a pilot-scale EPCM based TES system. For TES systems with EPCM, most of the experimental research have been focused on low temperature applications (Farid et al., 2004; Lane, 1976; IRENA, 2013; Nallusamy and Velraj, 2009), such as using encapsulated $CaCl_2{\cdot}6H_2O$ as a construction material for buildings' thermal management. There are very few process demonstrations being developed for high temperature applications, and most of the high temperature studies have been limited in the level of theoretical and computational studies (Dutil et al., 2011; Regin et al., 2008; Sharma et al., 2009; Verma et al., 2008). Therefore, it is essential to develop and execute the experimental verification of technical feasibility of the EPCM in test facilities. On one hand, it can be a demonstration to evaluate the technology viability before scale-up and commercialization. On the other hand, experimental testing data, such as stored energy and temperature profiles of EPCM, can be obtained to compare with model predictions to verify and adjust the mathematical model.

In the design of the EPCM based TES system, several parameters need to be determined: (1) Configuration of the EPCM based test section (T/S); (2) Physical dimensions of the test section; (3) Physical dimension, and number of the EPCM capsules; (4) Selection of HTF; and (5) Operating conditions of the HTF.

For determination of those parameters, a mathematical model is developed to analyze the effects of these parameters, and further optimize the test section design for desired performance. The key information of the model is described in the section below and more details are documented by Zheng (2015). There are four main criteria for quantification of these parameters: (1) Majority of the energy should be stored into or extracted from the PCM. In other words, the thermal masses of the other components are desired to be minimized. (2) The temperature drops of HTF should be large across the TES system, so that the errors for calculation of the total energy from the HTF will be small. Though air is used as the HTF, in this research, experiments are conducted with temperature

drops of the HTF higher than 20 °C considering the accuracy of the calibrated thermocouple (K-type) is within 0.4 °C. (3) All the encapsulated PCM will be preferred to complete phase change in a time period that is applicable for solar power plants. Considering the scale of current facility, the desired experiment duration is about 2–6 h for a charging/discharging process, and the experiment is ended when the temperature drop of the HTF decreases below 20 °C.

With considerations of many configurations, one-column inline system is chosen with heat transport fluid flowing across horizontally-oriented EPCM capsules. Following these design criteria, the mathematical model has been run to develop a set of those design parameters, including physical dimensions and operating conditions for desired test performance from EPCM capsules. It is found that the diameter of the capsule is one of the most important parameters. It is preferred to have a small diameter for the capsules considering that the thermal mass and conduction path will be small; while the EPCM will greatly contribute for the energy storage with a large diameter and a large amount of PCM mass. Through carefully analyzing multiple diameter options and manufacturing costs, the size of the cylindrical stainless steel capsules are selected to be constructed with a diameter of 76 mm, and a length of 254 mm. Considering the significant thermal expansion (Tufeu et al., 1985; Bauer et al., 2009), which is ~25% volume change for $NaNO_3$ for a temperature change from room temperature to 440 °C, the capsules were fabricated with an approximately 30% void space as an allowance for thermal expansion of $NaNO_3$. Considering thermal expansion of the PCM and the gas in the void, with the shell thickness of 1.6 mm, the shell is exposed to ~35 MPa tensile stress (Blaney et al., 2013).

The general layout of the test facility is shown in Fig. 1. The key component of the test loop is the vertical test section with ten EPCM capsules. The chamber of the test section is fabricated in rectangular, with a height of 1118 mm, a width of 93 mm and a length of 26 mm. The T/S is made of stainless steel 304 with a thickness of 3.175 mm which is chosen so that the relatively narrow T/S is strong enough to stand up without an external support. It is thin enough so that the thermal residue stored in it is minimized in the thermal charging and discharging process. The gap between the T/S surface and capsules is 8.3 mm, which has been minimized within the fabrication capabilities to provide a good contact area for the heat transfer between the HTF and the capsules. Considering the weight of the ten capsules in the T/S, In the test section, the ten EPCM capsules are separated into two stacks, with five capsules in the top section (capsules #1–#5) and the other five capsules in the bottom section (capsules #6–#10). For each stack, the bottom capsule is supported by the test section shell and the other four capsules sit on the supported capsule. In each stack, the capsule is horizontally orientated and sits on the lower one with their special-made square end plates. The overall test section is externally insulated with 150 mm thick mineral wool insulation to reduce its heat losses to the ambient.

Available HTFs, such as VP1 can only stand temperature up to 400 °C. The HTF is selected to be air in the current test facility for both charge and discharge the EPCM considering its flexibility over liquid HTFs. In a typical charging or discharging process, the air is preheated to a selected temperature by an external electric heater which is shown in Fig. 1(a), and flows from the top of the test section to transfer the heat to or extract the energy from the EPCM capsules. With the considerations of the expensive valves and the potential difficulties in their operations at high temperatures, the air is chosen to always be sent into the test section downwards, i.e., flow from the top of the T/S to the bottom in current demonstrations, so that a simulation model for the EPCM based test section can be verified first and capable of working further on the cases using different air flow directions (Zheng, 2015). In this test facility, the air can be operated in the range of 0.01–0.05 kg/s for its mass flow rate, and up to 600 °C for its temperature. To accommodate a 1–5 psi pressure drop across the flow distributors at the inlet and at the outlet of the test section, the air is slightly pressurized with ~20 psig pressure before the first EPCM capsule. At the outlet of the test section, the air still possess considerable heat and is hot, therefore, a cooler is assembled with spraying water inside to cool the air to 40–60 °C for safety before exhausting the air to the outside.

In order to demonstrate the energy storage within and retrieval from the encapsulated $NaNO_3$, it is necessary to measure the total energy stored in the capsules in the charging process and the total energy extracted from the capsules in the discharging process. For the material of $NaNO_3$, it is very difficult to determine its total energy change directly with temperature sensors, since it is hard to measure and identify the molten fraction or solidification fraction inside the capsules. However, the energy storage and retrieval of the encapsulated $NaNO_3$ capsules can be measured indirectly by subtracting the energy stored into the other components – chamber, insulation and heat losses, from the total energy from the HTF, as described below in Eq. (1).

$$Q_{Capsules}(t) = Q_f(t) - [Q_c(t) + Q_i(t) + Q_l(t)] \quad (1)$$

where t indicates the time; Q_f is the total energy exchanged between the TES system and the HTF; Q_c is the energy stored in the chamber of the TES system; Q_i is the energy stored in the insulation; and Q_l is the heat losses to the ambient at the outside surface of the insulation. And each of the energy term in the right-hand side of the Eq. (1) can be explored further as below for measurements:

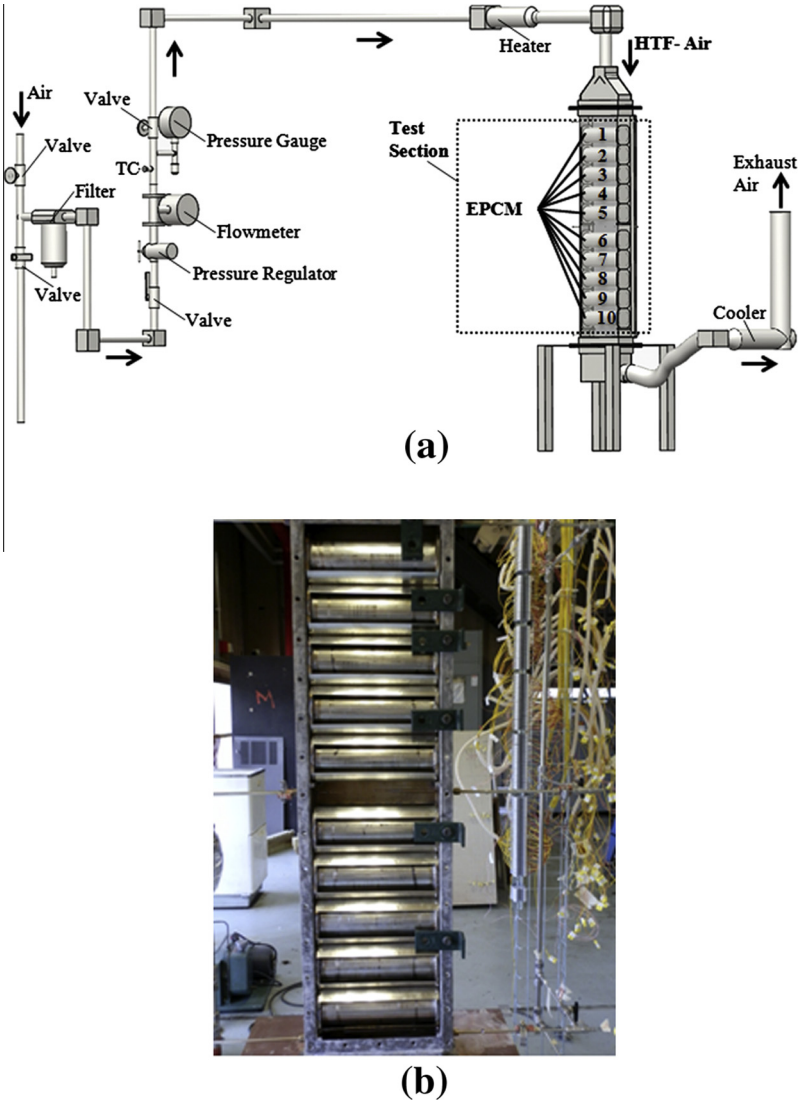

Fig. 1. The test facility with EPCM based TES system for process demonstration. (a) Schematic of the general test loop (without insulation); (b) a photo of the encapsulated $NaNO_3$ capsules in the test section.

$$
\begin{aligned}
Q_f(t) &= \int_{t_0}^{t} \dot{m}_f(t) C_{p,f}(T_{f,in}(t) - T_{f,out}(t))dt, \\
Q_c(t) &= \sum_{\mathrm{j}} m_{c,j} C_{p,c}(T_{c,t} - T_{c,t_0}) \\
Q_i(t) &= \sum_{\mathrm{j}} m_{i,j} C_{p,i}(T_{i,t} - T_{i,t_0}) \text{ and} \\
Q_l(t) &= \sum_{\mathrm{j}} \int_{t_0}^{t} \dot{Q}_{l,j}(t) \cdot A_{l,j} dt
\end{aligned}
\tag{2}
$$

With known thermal properties of the air, T/S chamber and insulation (Incropera and DeWitt, 2001; Zheng, 2015) the amount of energy captured by the components – HTF, T/S chamber, insulation and heat losses can be determined through measuring the other parameters in the Eq. (2), and further determine the total energy storage and retrieval of the $NaNO_3$ capsules by using Eq. (1).

For the total energy exchanged between the HTF and the TES system, the mass flow rates of the HTF $\dot{m}_f(t)$ are calculated with the measurements of its volumetric flow rate (m^3/s) before the heater with temperature and pressure compensations, as shown in Fig. 1. Thermocouples with aspirating subsystem are specially designed to measure the high temperature air flow at the inlet and at the outlet of the TES system. This aspirating subsystem consists of a stainless steel tube to cover the air thermocouple, and a pump to aspirate a specific amount of air out of the TES system. With delicate calculations and designs, the aspirating subsystem is effective to minimize the errors in measuring the high temperature air due to the radiation loss of thermocouples tips to the chamber surface, and it is expected to have the total energy of the HTF measured within ±2% errors with error analysis. Though about 20% of the energy from the air is lost through the insulation in

the experiment, T/Cs are located in 9 groups at selected locations and 7 depths of the insulation to establish heat transfer through the insulation, and 12 heat flux meters are located in 3 groups at selected locations to determine the heat losses at the surface of the insulation. It has been found that the energy storage and retrieval of the EPCM capsules can be measured within 5% errors with the measurement facilities, of which the details are discussed in the validation tests.

3. A mathematical model for the EPCM based TES system

For the numerical model, the overall height of the test section is denoted as Z [m]. The total length of test section is divided into N equal cells, where N equals the number of the EPCM capsules, and each cell contained one capsule. For each cell, energy balances are calculated for each component of the test section, i.e. HTF, EPCM capsules, T/S chamber, insulation and heat losses from the outside surface of the insulation, to investigate the transient heat transfer process during thermal charging and discharging cycles. Furthermore, the capsule and the PCM inside are radially divided to small meshes in order to calculate radial temperature variation as shown in Fig. 2(b). When the PCM inside the capsule reaches melting temperature, it is allowed to melt or solidify by adding the latent heat. As a result at any given time the capsule has three different layers: the solid shell, liquid PCM and a solid PCM. For simplicity of calculations, it is assumed that the solid PCM stays at the center of the capsule and there is no natural convection in the liquid PCM layer.

The heat conduction is assumed to be in the radial direction only, that is the temperature of the PCM, and the temperature of the shell is the function of time and radial location only as described by

$$\rho_{\mathrm{PCM}} C_{p,\mathrm{PCM}} \partial T_{\mathrm{PCM}}/\partial t = k_{\mathrm{PCM}}/r_{\mathrm{PCM}}[\partial(r_{\mathrm{PCM}}\partial T_{\mathrm{PCM}}/\partial r_{\mathrm{PCM}})/\partial r_{\mathrm{PCM}}] \tag{3}$$

$$\rho_s C_{p,s} \partial T_s/\partial t = k_s/r_s[\partial(r_s \partial T_s/\partial r_s)/\partial r_s] \tag{4}$$

While Eq. (3) only accounts for the heat conduction inside the PCM in its single phase, the energy balance in the interface between two phases is analyzed when the temperature of the PCM reaches its melting point as described by

$$\begin{aligned}&\rho_{\mathrm{PCM}}\Delta H_{\mathrm{PCM}} L_{Capsule} \times \pi[(S_{\mathrm{PCM}}(t))^2 \\ &\quad - (S_{\mathrm{PCM}}(t-\Delta t))^2]/\Delta t \\ &\quad = (k_{\mathrm{PCM}} A_{\mathrm{PCM}} \partial T_{\mathrm{PCM}}/\partial r_{\mathrm{PCM}})_{r_{\mathrm{PCM}}=S_{\mathrm{PCM}}-\Delta r_{\mathrm{PCM}},\mathrm{solid}} \\ &\quad - (k_{\mathrm{PCM}} A_{\mathrm{PCM}} \partial T_{\mathrm{PCM}}/\partial r_{\mathrm{PCM}})_{r_{\mathrm{PCM}}=S_{\mathrm{PCM}}+\Delta r_{\mathrm{PCM}},\mathrm{liquid}}\end{aligned} \tag{5}$$

In this equation, S_{PCM} is the distance of the interface (moving front) from the inside surface of the shell, as sketched in Fig. 2(c). It can be used as an indicator for the progress of the phase change – when its value is zero, it means that the PCM is 100% in single phase; when its value is equal to the radius of the PCM, it means that the PCM has completed the phase change. And the value of the displacement of the melting front can also be used to calculate the percentage of the molten fraction, and further decide the contribution of the phase change in the overall energy stored into and retrieved from the EPCM. As indicated in Fig. 2, the capsule is considered to be filled with the PCM having uniform density. Since the real capsule has a specific void space in the capsule as an allowance for PCM's thermal expansion, the density is adjusted accordingly in this model to ensure a constant mass. The density is assumed to be independent of the temperature, therefore during the phase change the solid PCM would stay in the center when liquid phase forms on the outside as shown in Fig. 2(c).

For the heat transfer fluid flowing across a specific zone of Δz, part of the total energy from the HTF is transferred to the capsule and T/S chamber by convection, while the other part is captured by the HTF itself in this section as described by

$$\begin{aligned}\rho_f C_{p,f} \partial T_f/\partial t = G_f C_{p,f} \partial T_f/\partial z - [h_s A_s (T_f - T_s)]_{r_s=R_s} \\ - [h_c A_c (T_f - T_c)]_{x_c=0}\end{aligned} \tag{6}$$

The convective heat transfer coefficient from the HTF to the surface of the capsule is calculated using Zhukauskas correlation (Zhukauskas, 1972) for the circular cylindrical in cross flow with the assumption that it is independent of the angular coordinate θ and length direction l. And

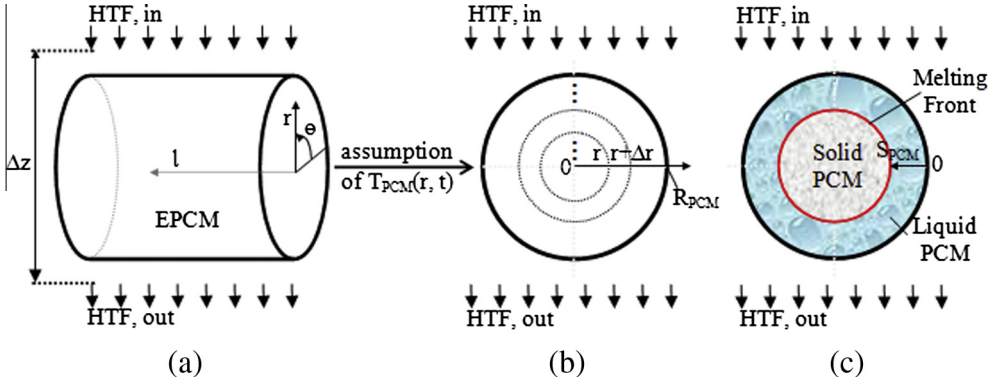

Fig. 2. The details of the model for an EPCM capsule in a specific elevation. (a) Temperature of PCM is a function of (r, θ, l, t) (front view); (b) temperature is dependent on the radial location r and time t in this model; (c) melting front inside the PCM during its phase change.

the average convective heat transfer coefficient from the HTF to the surface of the T/S chamber is also calculated using Zhukauskas correlation considering that with the current design, the flow of HTF at the surface of the T/S chamber is similar to the flow of HTF at the surface of the EPCM capsule. It is found that the effects of radiation is negligible with less than 2% of the convective heat transfer power according to calculation for current facility design.

One-dimensional model is applied for the inside heat conduction for the T/S chamber and insulation. Including a changing surface area for heat conduction from the inside surface of chamber to the outside surface of the insulation the energy equations are described by

$$(\rho_c C_{p,c}\partial T_c/\partial t)_{x_c} = (k_c A_c \partial T_c/\partial x_c)_{x_c-\Delta x_c} - (k_c A_c \partial T_c/\partial x_c)_{x_c+\Delta x_c} \quad (7)$$

$$(\rho_i C_{p,i}\partial T_i/\partial t)_{x_i} = (k_i A_i \partial T_i/\partial x_i)_{x_i-\Delta x_i} - (k_i A_i \partial T_i/\partial x_i)_{x_i+\Delta x_i} \quad (8)$$

At outside surface of insulation, natural convection is considered for the heat loss to the ambient with the heat transfer coefficient calculated using Churchill and Chu correlation (Churchill and Chu, 1975)

$$(\rho_i C_{p,i}\partial T_i/\partial t)_{x_i=\delta_i} = (k_i A_i \partial T_i/\partial x_i)_{\delta_i-\Delta x_i} - [h_a A_i (T_i - T_a)]_{x_i=\delta_i} \quad (9)$$

Finite difference method has been used to discretize Eqs. (7)–(9). The temperature profiles for each of the component – EPCM, HTF, T/S chamber and insulation can be obtained to determine the dynamic nature of the TES system. Especially for the EPCM capsules, it is of great value to further calculate their energy storage and retrieval during the thermal charging and discharging cycles. The results of the simulations will be compared against the experimental data.

4. Results

4.1. Validation

As described previously, the energy storage and retrieval of the $NaNO_3$ capsules can be determined from measured data. The question followed is how reliable are those facilities for measuring the energy change of the EPCM capsules using this methodology. To address this question, measurements have been conducted using solid copper capsules. The copper capsules are fabricated with the same dimensions and designs as EPCM capsules. There is a thermocouple well in the center of the capsule with a depth of the capsule radius for each of the copper capsule. During the thermal tests, a thermocouple is inserted into the end of the well to measure the center temperature of the copper capsule. Through simulations, it has been found that the temperature variation is smaller than 0.1 °C in every capsule with current operating conditions and capsule sizes. Therefore, the center temperature is well representative of the average temperature of the copper for each capsule.

With known thermal properties of copper (Incropera and DeWitt, 2001), the energy stored in the copper capsules $Q_{Copper}(t)$ can be determined by using measured temperature as

$$Q_{Copper}(t) = \sum m_c C_{p,c}(T_{c,t} - T_{c,t_0}) \quad (10)$$

The energy stored in the copper capsules can also be determined from the energy balance described in Eqs. (1) and (2). Examining the difference in the energy storage determined by these two approaches can help validating the experimental techniques utilized here. The thermal responses for each of the components in the test section have been recorded, as shown in Fig. 3 for the key information in a typical charging process. It is seen that the inlet air, with a mass flow rate of 0.038 kg/s, have been well maintained at high temperature 440 °C after a short transient process due to the preheating of the piping and insulation between the furnace and TES system. The temperature drop of the air across the system, that is, the temperature difference between the inlet air and outlet air, decreases with the time when the test section is being thermally charged. The #1 copper capsule near the inlet has been heated up quickly and its temperature is close to the inlet air temperature within one hour. Compared with the #1 copper capsule, the #10 copper capsule located near the outlet is heated up slower since the air flow is cooler on the outside surface of the capsule in the lower section. At the end of the testing, the temperatures of the ten copper capsules are in the range of ~360 °C to 425 °C, and with about 65 °C temperature difference between the capsules near the inlet and near the outlet. Besides the temperature history of the copper capsules and air flow, Fig. 3(c) also shows an example for a group of insulation temperature from the outside surface of the T/S chamber to the outside surface of the insulation at the midway of the test section. It is seen that the temperatures of the insulation increase following the similar trend as the copper capsule's, with the surface of the chamber at ~380 °C and the outside surface of the insulation slightly higher than room temperature at the end of this charging process. For the heat flux at the outside surface of the insulation, it is seen that it increases from ~+2 W/m^2 to ~+12 W/m^2, see Fig. 3(d). The positive sign means that the heat losses are from the insulation surface to the ambient.

The air mass flow rates, and its temperature drops across the test section are integrated over the time to calculate the total energy from the air as indicated in Eq. (2). The temperatures at the outside surface of chamber are used to calculate the energy captured by the test section itself, with the assumption of a linear temperature change along the elevation direction. The energy residue in each layer of the insulation has been calculated with the

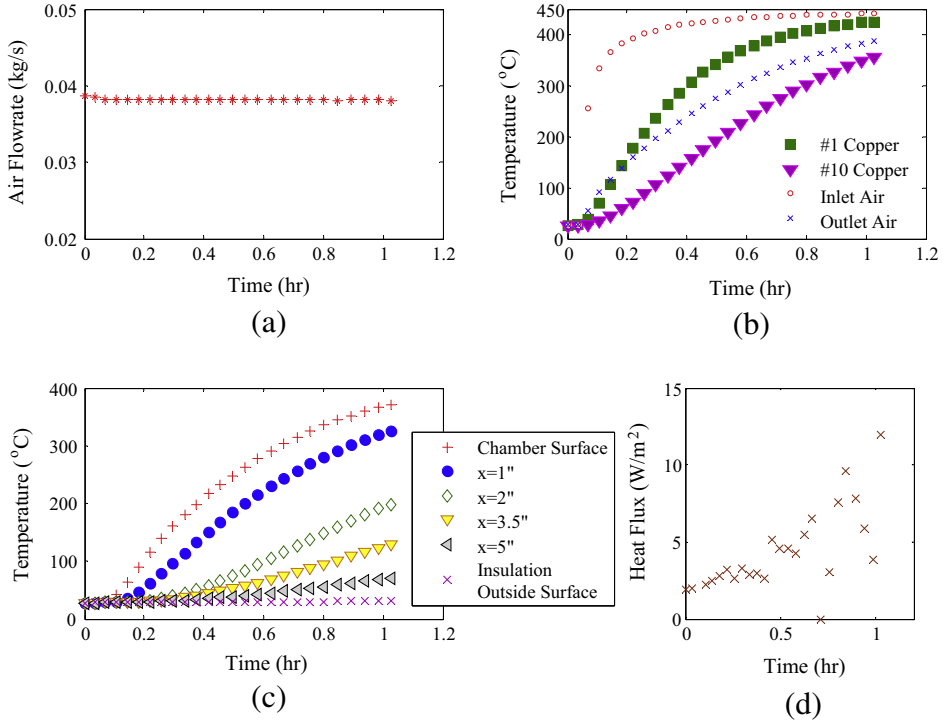

Fig. 3. Key information for a verification test with copper capsules in a typical charging process. (a) Mass flow rate of HTF – air; (b) temperature history of the copper capsules and air; (c) insulation temperatures from chamber surface to outside surface at midway of the test section; (d) heat flux on the outside surface of the insulation at the midway of the storage system.

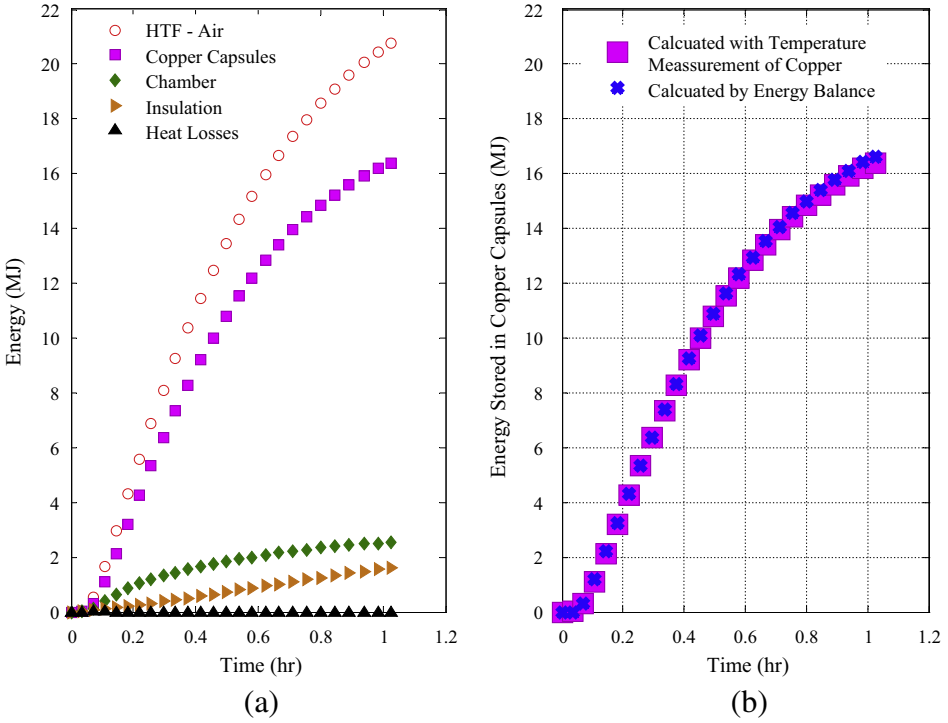

Fig. 4. Energy storage of the TES system in a charging test. (a) Energy storage by every component from measurements. (b) Energy stored in copper capsules calculated in two ways.

assumptions of linear temperature change between the measurements of the two layers and along the elevations directions. The heat losses at the outside surface are calculated by integrating the heat flux over the experimental time for a certain surface area with the assumption that a uniform heat flux (W/m^2) in this area. The total energy from the air, the energy stored in the chamber and insulation, and the heat losses are shown in Fig. 4(a) in the charging test with copper capsules. From this figure, it is seen that at the end of the experiment, there is ~22 MJ energy transferred from the air to the overall test section, of which ~20% is stored into the chamber and insulation, and a negligible part is the heat losses to the ambient.

The total energy stored in the copper capsules that is calculated with the measurements of the copper temperatures is shown by purple solid squares in Fig. 4(a) and (b). The stored energy that is calculated by the energy balance is denoted by the blue[1] crosses in Fig. 4(b). It is seen that the energy measurements of the copper capsules from these two methods are in a very good agreement, with a ~1% discrepancy at the end of this charging test. The verification tests have been carefully conducted by testing the copper capsules in multiple thermal cycles. The total energy stored in the charging process, and the total energy extracted in the discharging process have been analyzed for the tested copper capsules in different temperature ranges as tabulated in Table 1. The energy change of the copper capsules that is calculated by two methods is listed in Table 1. It is seen that the difference are within ±5% in various test ranges, which is leading confidence to the experimental method and measurements in determination of the energy storage of the capsules in the test section.

4.2. Performance tests of the $NaNO_3$ capsules in thermal cycles

The thermal energy storage and retrieval of the $NaNO_3$ capsules are analyzed to demonstrate the viability of the storage technology for thermal energy using encapsulated phase change materials. As described previously, the energy stored in the $NaNO_3$ capsules is calculated by the energy balance with all the verified measurement facilities. Meanwhile it is also essential to monitor the thermal behavior of the $NaNO_3$ in the charging and discharging process, therefore a thermocouple is placed in the last capsule to track the temperature of the $NaNO_3$ near the outlet of the test section. As indicated in Fig. 5, this thermocouple measures the temperature of the $NaNO_3$ at the very bottom of the capsule, where the temperature indicates the possible lowest temperature of the $NaNO_3$ in a charging process, and the higher temperature in a cooling process in the current test section. Choosing this measurement point and this length of the TC well is also based on the consideration to avoid the break-down of the TC well from the hanging of the solid $NaNO_3$ when liquid phase $NaNO_3$ is formed from outside shell of the capsule.

Fig. 6 shows the temperature history of the air and the $NaNO_3$ near the outlet of the T/S when the test section is heated up from room temperature. The inlet temperature of air, the HTF, is chosen to be 440 °C to gather information up to temperatures much higher than melting point of $NaNO_3$. It is seen that during the charging run, the temperature increase of the $NaNO_3$ significantly slows down when it is approaching to its melting point, 308 °C. After the $NaNO_3$ completely melts, the $NaNO_3$ is superheated quickly in the liquid phase to ~380 °C at the end of this charging process. In the discharging process, the $NaNO_3$ cools down quickly with a sharp turn as its temperature decreases below the freezing point. One of the reasons for the appearance of the longer melting process is because the cold solid sodium nitrate sinks and touches the thermocouple.

Fig. 7 shows the total energy stored in the 10 $NaNO_3$ capsules in this thermal cycle. Cumulative energy content of all capsules is shown on the vertical axis in reference to energy content at room temperature. It is seen that ten capsules can store a cumulative energy of 18.3 MJ when the temperature of the bottom capsule reaches 386 °C. At this time the capsules #1–#9 are at higher temperatures up to 440 °C because the temperature of #1 capsule near the inlet is expected to approach the temperature of inlet air. From this experimental data, one sample case is calculated for CSP applications, which assumes the temperature change for the bottom capsule from 250 °C to 386 °C. It is seen that the 10 $NaNO_3$ capsules successfully capture 7.34 MJ energy while the temperature of the bottom capsule rises from 250 °C to 386 °C. Then in the continued discharging process, the total energy retrieved from the capsules is ~10.1 MJ while the temperature of the bottom capsule cools down from 386 °C to 250 °C. The energy retrieved is higher than the stored energy because at the beginning of the retrieval process (end of the charging process) all nine capsules above the bottom capsule are at higher temperatures than the bottom capsule, and at the end of the retrieval process (when the bottom capsule is again cooled back to 250 °C) all of the capsules above the bottom capsule are at lower temperatures then the bottom one. Furthermore, the total stored or retrieved energy by the PCM can be estimated by using inlet and outlet temperatures of the HTF (air) as follows: for the charging process, if we assume the temperature of the capsule shells #1 and #10 to be the same as the air at the inlet and at the outlet, respectively. Then one can assume a linear temperature change from the #1 to #10 capsule shells with uniform temperature inside the each thin capsule shell, the total energy stored into the capsule shells can be estimated. Subtracting this estimated energy stored by the capsule shells from the measured total energy storage of EPCM capsules, the 17.7 kg sodium nitrate PCM would expect to store approximately 7.0 MJ energy when the bottom

[1] For interpretation of color in Figs. 4 and 12, the reader is referred to the web version of this article.

Table 1
Measurements of energy storage and retrieval in the verification tests with multiple thermal cycles.

Verification test	Temperature range of copper capsules (°C)	Energy stored in/retrieved from the copper capsules (MJ)		Difference percentage (%)
		Calc. by energy balance	Calc. by copper temperature change	
Heating #1	27–425	16.54	16.38	1.0
Cooling #2	425–65	13.37	13.26	0.8
Heating #3	65–421	13.05	12.82	1.8
Cooling #4	421–148	8.34	8.16	2.2
Heating #5	148–421	9.04	8.62	4.9
Cooling #6	421–53	14.25	14.05	1.4
Heating #7	281–431	9.67	9.83	−1.6
Cooling #8	431–47	15.82	15.79	0.2
Heating #9	47–426	15.19	15.24	−0.3

#10 capsule is heated from 250 °C to 386 °C, that is, an average of ~395 kJ energy stored in per unit mass of the encapsulated $NaNO_3$. With the measurement facilities, the ten $NaNO_3$ capsules are found to store ~211 kJ per kg of the capsules, of which the latent heat contributes to more than 42% of the total energy stored in the capsules. The storage capacity [kJ/kg] of encapsulated $NaNO_3$ is expected to be even higher with a larger capsule or larger scale test section without the penalties associated with current limited test facility.

The storage capacity [kJ/kg] of encapsulated $NaNO_3$ is expected to be even higher with a larger capsule or larger scale test section without the penalties associated with current limited test facility.

Besides the storage capacity of the EPCM capsules, the rate of energy storage and removal is another key parameter for evaluation of the storage performance EPCM capsules. The rate of storage is related to: the thermal properties of the storage materials, the heat transfer rates from the HTF to the capsules, the properties of the heat transfer fluid, and EPCM capsules and capsules' geometry. In the experiment, the rate of the energy storage and removal is obtained by calculating the derivative of the energy stored in the $NaNO_3$ capsules over the time of thermal testing, which are shown in Fig. 8.

As shown in Fig. 8, the rate of the energy storage increases quickly first and reaches to a maximum of 6 kW, and then slows down and decreases to ~1 kW at the end of the charging process when the most of test section is cooled down to room temperature. In the discharging process, since the energy left in the capsules decreases the rate of the energy storage for the capsules is negative, as depicted in Fig. 8. It is seen that the absolute value of the rate of the energy storage in the cooling process has a similar trend. Within the temperature range of interest for $NaNO_3$ at ~250 °C to 440 °C shown previously in Fig. 6, it is seen that the rate of energy storage slowly decreases from 3.4 kW to 0.8 kW with the $NaNO_3$ came across its phase change in the charging process. In the discharging process, the absolute value of energy removal decreases from its maximum ~6 kW to ~3.6 kW in the discharging process as the temperature of #10 $NaNO_3$ drops to 250 °C. In this figure, it is also shown that the maximum of the rate of the energy storage or removal does not occur at the very beginning of the process. The maximum temperature difference between the air and the capsules occurs after the transient as the air temperature settles. With the current test facility, the average of the energy storage and removal is about 2 kW, which corresponding to a ~50 °C temperature difference between the air and capsules with the capsules surface area ~1 m^2 and an estimated 40 W/m^2 °C for the convective heat transfer coefficient. It has been expected based on the simulation work (Zheng, 2015) that the rate of the energy storage and removal

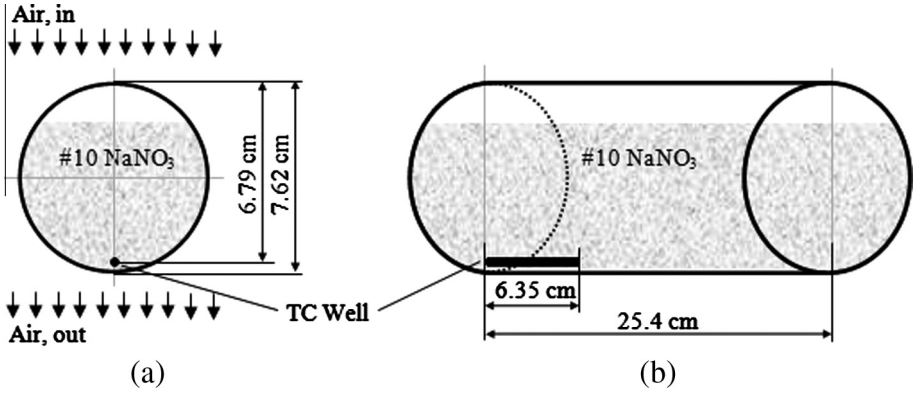

Fig. 5. The thermocouple location in the #10 $NaNO_3$ (not at scale). (a) Side view; (b) front view.

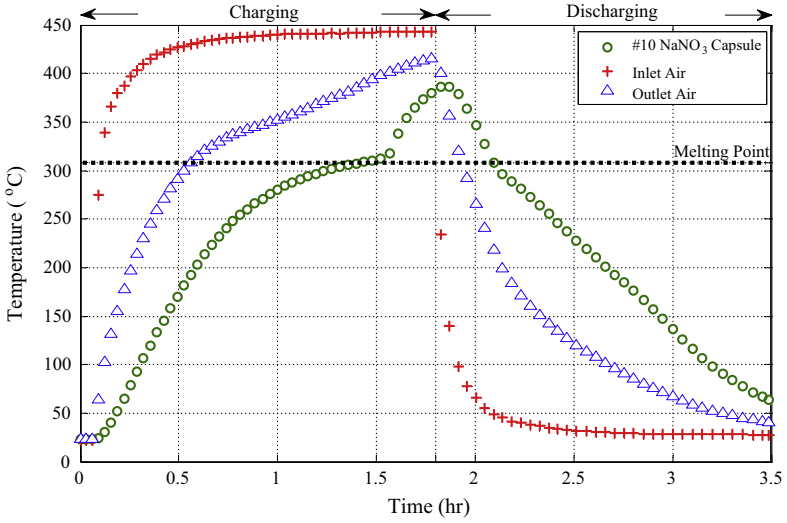

Fig. 6. The temperature history of the $NaNO_3$ near the outlet, and the air at the inlet and at the outlet of the test section in a thermal cycling.

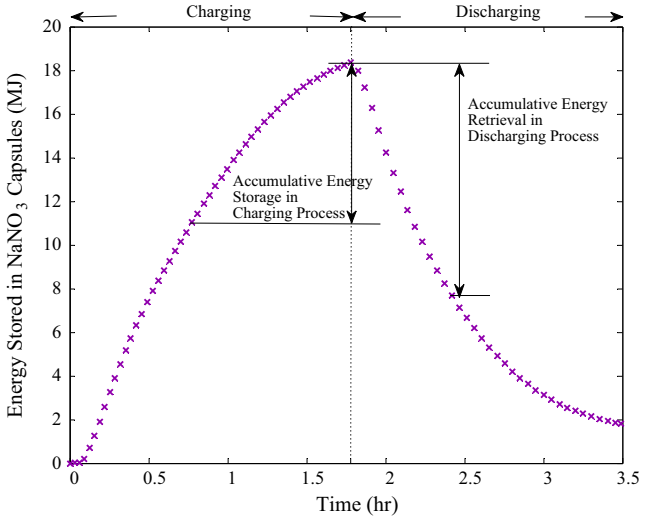

Fig. 7. The energy stored in the ten $NaNO_3$ capsules in a thermal cycling.

would be greater by using liquid HTF with which the convective heat transfer coefficient to the EPCM capsules would be significantly larger.

From the first thermal cycle test, it has been well demonstrated that the $NaNO_3$ capsules based test section can successfully store and retrieve thermal energy up to 440 °C, with phase change at its melting point 308 °C. The next question to address is how the behavior of encapsulated $NaNO_3$ is in multiple thermal cycles. With regards to the overall test section, it is necessary to examine the energy storage performance of the $NaNO_3$ capsules over several thermal cycles. It is of great importance to investigate the thermal behavior the PCM in thermal cycling, and ensure its compatibility with the encapsulation materials in current scale size and design. Therefore, in this experiment, the test section is tested with continuous charging and discharging processes. Fig. 9(a) shows the temperature history of the encapsulated $NaNO_3$ in three thermal cycles. The test section is charged by the hot air at ~440 °C, and discharged by the cool air at ~25 °C at the three heating processes and three cooling processes. In order to ensure the thermal behavior of the encapsulated $NaNO_3$, the charging process is always ended after the measured temperature for the $NaNO_3$ is above its melting point. The discharging processes are ended at different point with the $NaNO_3$ cooled down at different temperatures and re-charged up with various initial states. As shown in Fig. 9(a), the $NaNO_3$ at the #10 capsule is heated up from room temperature to ~400 °C in the first charging process, and then cooled down to ~50 °C at the end of the first cycle. In the second and third cycles, it is recharged to ~400 °C high temperature, and cooled down to ~100 °C at the end of that cycle. It is seen that the measured temperature trace of the $NaNO_3$ follows the same trend in the melting and solidification respectively during these three thermal cycles, which indicates a sustained thermal behavior of the encapsulated $NaNO_3$ in the current test runs. Meanwhile, it is seen that the air temperature at the outlet also follows similar traces between the three heating process and three cooling process, which demonstrate the stable behavior of the energy storage and retrieval of the overall test section under multiple thermal tests in different temperature ranges. With the measurement facilities, the amount of the energy stored into and retrieved from the 10 $NaNO_3$ capsules is quantified and plotted in Fig. 9(b) for each of the thermal tests. It is seen that the encapsulated $NaNO_3$ capsules can continuously store and release the thermal energy during the thermal cycle, and the current measurement facility shows its capability in measuring the energy storage and retrieval with various initial conditions of the T/S and transient heat transfer processes.

Take heating #2 and cooling #2 as an example, the $NaNO_3$ capsules capture about 17.5 MJ thermal energy from the air with their temperature raised from ~50 °C to ~440 °C, and relieve about 16 MJ thermal energy when the capsules are cooled from ~440 °C to ~100 °C. The differences between the amounts of the energy stored and

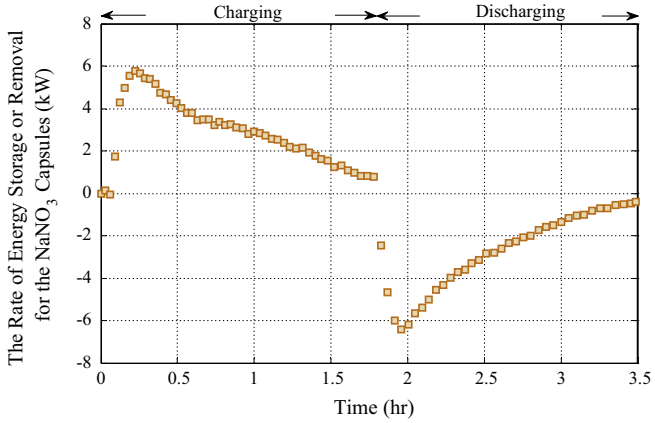

Fig. 8. The rates of energy storage and retrieval of the 10 $NaNO_3$ capsules in current test facility in a typical thermal charging and discharging cycle.

retrieved are from the operating temperature change and the progress of the phase change in the 10 $NaNO_3$ capsules. Comparison of the cooling process in previous thermal cycle and the heat process in current thermal cycle, for example cooling #2 and heating #3, through the measured $NaNO_3$ temperature shows that it is running at a quite close temperature range. The energy stored into the capsules is slightly higher than the energy extracted from the capsules, which might due to a more uniform temperature distribution in each capsule with the progress of the continuous thermal cycles. In that case, the average temperature in each capsule at the end of the heating #3 would be higher than the one at the end of the heating #2 (the beginning of the cooling #3).

This test section with 10 encapsulated $NaNO_3$ has been tested four times in 45 days with ~10 h of thermal cycles every time as shown in Fig. 9. After the 45 days, a charging test is conducted with the same operating conditions (inlet air temperature and mass flow of the air) as its first charging process for the $NaNO_3$ capsules as shown in Fig. 10(a), to repeat the experiment and investigate whether or not the energy storage is sustained after the $NaNO_3$ is encapsulated in the stainless steel capsule for 45 days and subject to occasional thermal test with ~40 h in thermal charging and discharging. In Fig. 10, it has been found that the temperature trace and the energy storage performance of the $NaNO_3$ capsules are consistent with ones in first charging test. And for the energy stored in the 10 $NaNO_3$ capsules, the discrepancy between the two tests is ~2.5% within the accuracy of the measurements in current test facility. It can be concluded that the encapsulated $NaNO_3$ capsules have sustained storage performance without the deterioration in their storage performance in current test range.

4.3. Comparison of the experimental data with predicted results for $NaNO_3$ tests

Simulations have been conducted for charging and discharging processes with $NaNO_3$ capsules. This is aimed to compare the experimental data with the simulation results, to investigate the capability of the model, and to improve performance the model if necessary for more accurate predictions. The mathematical model is also used to investigate the dynamics of the EPCM in the T/S during thermal cycles.

The model uses the measured mass flow rates of the air and the temperature of the air at the inlet as inputs. The temperature profiles of the $NaNO_3$ and insulation at various locations and the air temperature at the outlet are predicted.

Fig. 11 shows the predicted and measured air temperature and the temperature of $NaNO_3$ in a typical thermal cycle. For the temperature of $NaNO_3$ at the specific measurement point, there is a very good agreement between the experimental data and simulation results before the melting point of the $NaNO_3$ in the charging process, but a considerable difference is shown as the temperature is approaching the melting point. This difference is reasonable considering that in the experiment, thermocouple contacts with the colder solid $NaNO_3$ which is sinking to the TC location as PCM melts. The model makes the unrealistic but computationally efficient and practical assumption that the solid $NaNO_3$ stays in the center without sinking. Therefore, the simulation shows higher values than the experimental measurements when the melting process starts.

This is confirmed with the temperature profiles at other radial locations in the #10 $NaNO_3$ capsule predicted by the model, as shown in Fig. 12. The red dash line shows the temperature history of the $NaNO_3$ at the inside surface of the capsule $r = R_{PCM}$. It is seen that the deviation between the experiment measurements and simulation results for the measurement points appears at the time of $t = t_1$ when the $NaNO_3$ at the $r = R_{PCM}$ starts melting; while with the liquid $NaNO_3$ formed at this time from the outside shell, the solid $NaNO_3$ sink to the bottom in the realistic operating system, therefore a lower temperature is sensed in the experiment. At the end of the charging process $t = t_2$, the measured temperature for the $NaNO_3$ agrees with the predicted temperature at the inside surface of the capsule. This implies that a well-mixed $NaNO_3$ bulk is present during the melting process due to the natural convection.

The temperature of the air at the outlet has been well predicted at the beginning of the charging process when the $NaNO_3$ is in its solid phase, as shown in Fig. 11. The model overestimates the outlet temperature as $NaNO_3$ approaches the melting point. In other words, the temperature drop of the air across the T/S is slightly underestimated during this time. This may be due to the assumption of no natural convection in the liquid phase of the $NaNO_3$. For the discharging process with the solid $NaNO_3$ solidified from the surface of the capsule, it is seen that the outlet air temperature and the measured $NaNO_3$ temperature have been both well predicted by the model.

When summing up the energy stored in the each single capsule, the total energy stored in the 10 $NaNO_3$ capsules

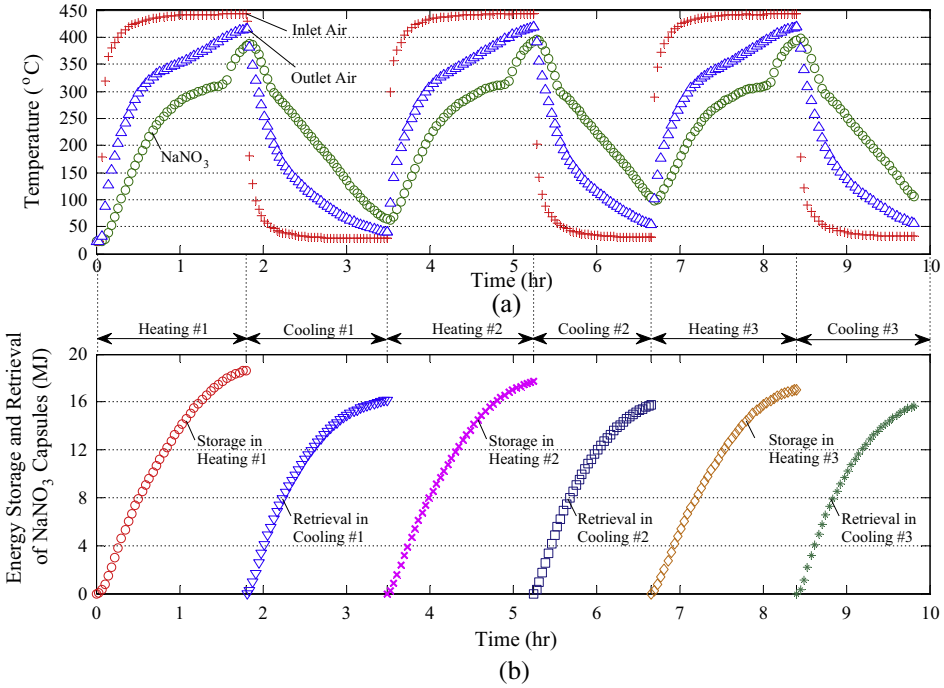

Fig. 9. Test of the $NaNO_3$ capsules in three continuous thermal charging and discharging processes. (a) Temperature history of the #10 $NaNO_3$ and air; (b) energy storage and retrieval of the encapsulated sodium nitrate capsules.

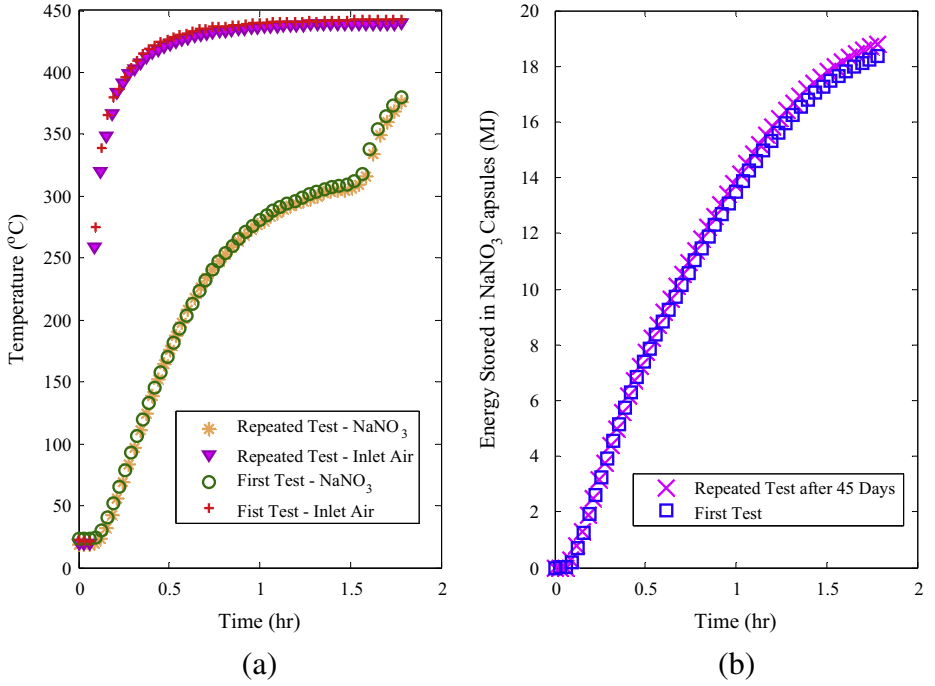

Fig. 10. Storage performance of the $NaNO_3$ capsules with the same operating conditions as the first charging process after 45 days. (a) Temperature profiles of the $NaNO_3$ and inlet air; (b) energy stored in the 10 $NaNO_3$ capsules.

can be obtained, as shown in Fig. 13. It is seen that the experimental measurements for the energy stored in $NaNO_3$ capsules have been well predicted at the beginning of the charging, when the $NaNO_3$ is mostly in solid phase. The difference appears especially after time = ~0.8 h when the encapsulated $NaNO_3$ are undergoing melting process. At the end of the charging process, the difference between the prediction and experimental measurement is approximately 7% for the energy stored in the 10 $NaNO_3$ capsules. As discussed previously, one of the reasons for the discrepancy is that the model neglects the natural convection and the sinking of the solid. It has been reported

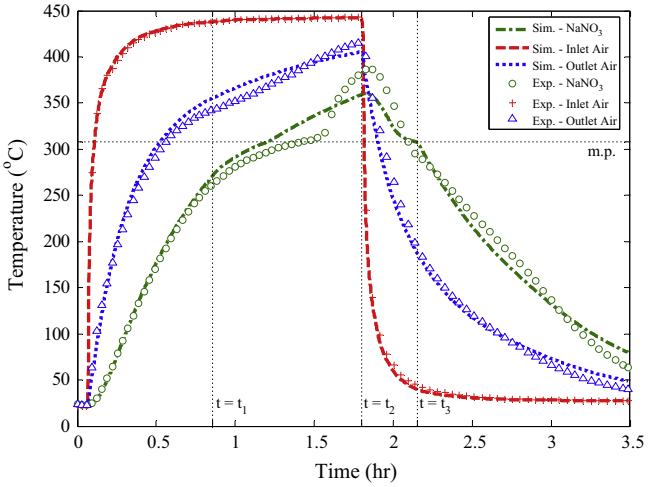

Fig. 11. The temperature of $NaNO_3$ and air temperature in a typical charging and discharging process.

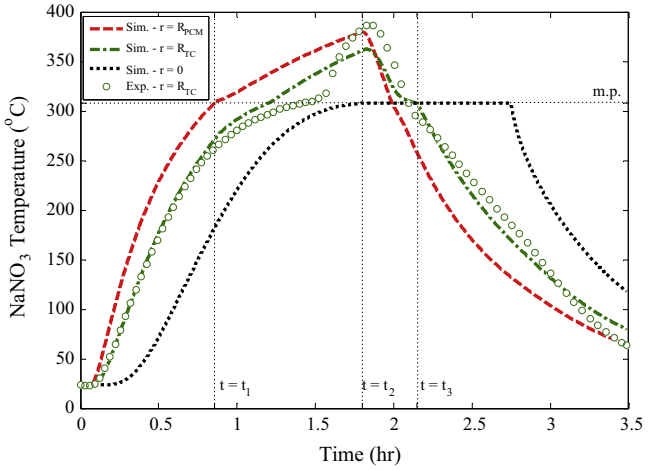

Fig. 12. The temperature of $NaNO_3$ in various radial locations in #10 capsule.

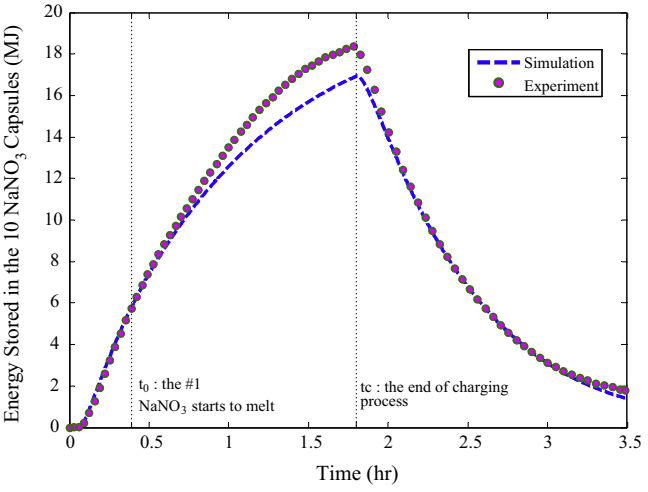

Fig. 13. The energy stored in the 10 $NaNO_3$ capsules in a thermal cycle.

that for a single encapsulated $NaNO_3$ capsule heating up by the 400 °C air, the time for the phase change would be shortened by ~10% if the gravity and natural convection is considered (Zhao, 2013). But our case is more complicated with multiple EPCM capsules with the air flowing at different temperatures along the T/S. The present authors are exploring the effects of gravity and the natural convections on the performance of the EPCMs.

5. Conclusions and summary

In this research, a pilot-scale test section is designed and built to demonstrate latent heat based thermal energy storage using EPCM in the temperature range of 250–386 °C for the bottom capsule. $NaNO_3$ is selected as the storage medium and is encapsulated in stainless steel. Multiple encapsulated $NaNO_3$ capsules are installed in the test section for the demonstrations of the energy storage and retrieval with phase change in thermal cycles. The test section is initially qualified using solid copper capsules and then loaded with encapsulated $NaNO_3$ capsules for performance test. A numerical model is developed to investigate the dynamic performance of the charging and discharging of the test section with phase change in the $NaNO_3$ capsule.

The experimental and the numerical investigations indicate that: (1) the test section with $NaNO_3$ capsules successfully demonstrated its ability to transfer thermal energy to and from a transport fluid, achieving energy storage and retrieval in multiple charging and discharging cycles. (2) In a given storage – retrieval cycle where the bottom capsule temperature varied from ~250 °C to ~386 °C, the test section has been found to store significant amounts of thermal energy in the EPCM capsules (~211 kJ/kg), with the $NaNO_3$ material (PCM) accounting for ~95% of the energy stored in the capsules. The latent heat of phase change of the $NaNO_3$ contributed significantly to ~42% of the energy stored in the capsules, providing high storage density. (3) A thermal energy storage test has been conducted after the $NaNO_3$ capsules have been tested ~40 h in 45 days. It has been found that the encapsulated $NaNO_3$ capsules have sustained storage performance without deterioration in their storage capacity. (4) The results of the numerical simulations of the energy storage are found to agree with experimental measurements within 7%. The dynamic performance of charging and discharging rates were also well predicted by the model, giving confidence for engineering design capabilities in future applications using encapsulated phase change materials for energy storage. Further research work in this area could include the effects of multiple PCMs, the fluid temperature swings and the importance of gravity and natural convection in large EPCM based thermoclines.

Acknowledgements

We thank Matthew Bernstein, John Caffrey, Paul N. Bader and William Maroun for their help during the

fabrication of the test facility. We gratefully acknowledge the support extended by U.S. DOE per award DE-FG36-08GO18050 for the present work.

References

Bauer, T., Laing, D., Kröner, U., Tamme, R., 2009. Sodium nitrate for high temperature latent heat storage. In: The 11th International Conference on Thermal Energy Storage - Effstock, 14–17 June 2009, Stockholm, Sweden.

Blaney, J.J., Neti, S., Misiolek, W.Z., Oztekin, A., 2013. Containment capsule stresses for encapsulated phase change materials. Appl. Therm. Eng. 50, 555–561.

Churchill, S.W., Chu, H.H.S., 1975. Correlating equations for laminar and turbulent free convection from a vertical plate. Int. J. Heat Mass Transf. 18, 1323–1329.

Dinter, F., Geyer, M.A., Tamme, R., 1991. Thermal Energy Storage for Commercial Applications: A Feasibility Study on Economic Storage Systems, first ed. Springer-Verlag Berlin Heidelberg.

Dunn, R.I., Hearps, P.J., Wright, M.N., 2012. Molten-salt power towers: newly commercial concentrating solar storage. Proc. IEEE 100, 504–515.

Dutil, Y., Rousse, D.R., Ben Salah, N., Lassue, S., Zalewski, L., 2011. A review on phase-change materials: mathematical modeling and simulations. Renew. Sust. Energy Rev. 15, 112–130.

Energy Information Administration, 2012a. Annual Energy Outlook 2012.

Energy Information Administration, 2012b. Electric Power Monthly.

Farid, M.M., Khudhair, A.M., Razack, S.A.K., Al-Hallaj, S., 2004. A review on phase change energy storage: materials and applications. Energy Convers. Manage. 45, 1597–1615.

Incropera, F.P., DeWitt, D.P., 2001. Fundamentals of Heat and Mass Transfer, fifth ed. John Wiley & Sons Inc..

IRENA, 2013. Thermal Energy Storage Technology Brief.

Kuravi, S., Trahan, J., Goswami, D.Y., Rahman, M.M., Stefanakos, E.K., 2013. Thermal energy storage technologies and systems for concentrating solar power plants. Prog. Energy Combust. Sci. 39, 285–319.

Laing, D., Bauer, T., Breidenbach, N., Hachmann, B., Johnson, M., 2013. Development of high temperature phase-change-material storages. Appl. Energy 109, 497–504.

Lane, G.A., 1976. Macro encapsulation of heat storage phase change materials for use in residential buildings. Dow Chemical Company, Final Report 1976.

Luz International Ltd., Solar Energy Research Institute, CBY Associates, I., 1988. Phase-Change Thermal Energy Storage. SERI/STR-250-3516.

Metz, B., Davidson, O., Coninck, H.D., Loos, M., Meyer, L., 2005. IPCC special report on carbon dioxide capture and storage. Cambridge University Press, New York, United States of America.

Michels, H., Pitz-Paal, R., 2007. Cascaded latent heat storage for parabolic trough solar power plants. Sol. Energy 81, 829–837.

Nallusamy, N., Velraj, R., 2009. Numerical and experimental investigation on a combined sensible and latent heat storage unit integrated with solar water heating system. J. Solar Energy Eng. – Trans. ASME 131, 041002-1–041002-8.

Pacheco, J.E., Showalter, S.K., Kolb, W.J., 2002. Development of a molten-salt thermocline thermal storage system for parabolic trough plants. J. Sol. Energy Eng. 124 (2), 153–159.

Regin, A.F., Solanki, S.C., Saini, J.S., 2008. Heat transfer characteristics of thermal energy storage system using PCM capsules: a review. Renew. Sust. Energ. Rev. 12, 2438–2458.

Sharma, A., Tyagi, V.V., Chen, C.R., Buddhi, D., 2009. Review on thermal energy storage with phase change materials and applications. Renew. Sust. Energ. Rev. 13 (2), 318–345.

Steinmann, W., Laing, D., Tamme, R., 2010. Latent heat storage systems for solar thermal power plants and process heat applications. J. Solar Energy Eng. – Trans. ASME 132, 021003.

Tufeu, R., Petitet, J., Deniellou, L., Leneindre, B., 1985. Experimental determination of the thermal conductivity of molten pure salts and salt mixtures. Int. J. Thermophys. 6, 315–330.

Verma, P., Varun, Singal, S.K., 2008. Review of mathematical modeling on latent heat thermal energy storage systems using phase-change material. Renew. Sust. Energy Rev. 12, 999–1031.

Zhao, W., 2013. Characterization of Encapsulated Phase Change Materials for Thermal Energy Storage. PhD Dissertation, Lehigh University, Bethlehem PA, USA.

Zhao, W., Zheng, Y., Sabol, J.C., Oztekin, A., Neti, S., Tuzla, K., Misiolek, W.M., Chen, J.C., 2012. Heat transfer analysis for thermal energy storage using $NaNO_3$ as encapsulated phase change Material. In: ASME 2012 Heat Transfer Summer Conference, July 8–12 2012, Puerto Rico, USA.

Zheng, Y., 2015. Thermal Energy Storage with Encapsulated Phase Change Materials for High Temperature Applications. PhD Dissertation, Lehigh University, Bethlehem PA, USA.

Zheng, Y., Zhao, W., Sabol, J.C., Tuzla, K., Neti, S., Oztekin, A., Chen, J.C., 2013. Encapsulated phase change materials for energy storage – characterization by calorimetry. Sol. Energy 87, 117–126.

Zhukauskas, A., 1972. Heat transfer from tubes in cross flow. In: Hartnett, J.P., Irvine, T.F. (Eds.), Advances in Heat Transfer. Academic Press, New York.